



PERGAMON

Available online at [www.sciencedirect.com](http://www.sciencedirect.com)

SCIENCE @ DIRECT®

Planetary and Space Science 50 (2002) 1345–1353

Planetary  
and  
Space Science

[www.elsevier.com/locate/pss](http://www.elsevier.com/locate/pss)

## The SMART-1 X-ray solar monitor (XSM): calibrations for D-CIXS and independent coronal science

J. Huovelin<sup>a,\*</sup>, L. Alha<sup>a</sup>, H. Andersson<sup>c</sup>, T. Andersson<sup>b</sup>, R. Browning<sup>e</sup>, D. Drummond<sup>e</sup>, B. Foing<sup>g</sup>, M. Grande<sup>e</sup>, K. Hämäläinen<sup>b</sup>, J. Laukkanen<sup>b</sup>, V. Lämsä<sup>c</sup>, K. Muinonen<sup>a</sup>, M. Murray<sup>d</sup>, S. Nenonen<sup>c</sup>, A. Salminen<sup>c</sup>, H. Sipilä<sup>c</sup>, I. Taylor<sup>d</sup>, O. Vilhu<sup>a</sup>, N. Waltham<sup>e</sup>, M. Lopez-Jorkama<sup>f</sup>

<sup>a</sup>*Observatory, University of Helsinki, P.O. Box 14, FIN-00014 Helsinki, Finland*

<sup>b</sup>*X-ray Laboratory, Department of Physics, P.O. Box 9, FIN-00014 Helsinki, Finland*

<sup>c</sup>*Metorex International Oy, P.O. Box 85, FIN-02631 Espoo, Finland*

<sup>d</sup>*Metorex Inc., Princeton Crossroads Corporate Center, 250 Phillips Boulevard, Ewing, NJ 08618, USA*

<sup>e</sup>*Rutherford Appleton Laboratory, Chilton, Didcot, Oxon, OX11 0QX, UK*

<sup>f</sup>*VTT Automation, P.O.Box 1303, FIN-02044 VTT, Finland*

<sup>g</sup>*ESA Space Science Department, ESTEC/SCI-SO, Postbus 299, 2200 AG Noordwijk, The Netherlands*

Accepted 27 June 2002

### Abstract

The X-ray solar monitor (XSM) is a calibration instrument of the demonstration of compact imaging X-ray spectrometer (D-CIXS) experiment, with a separate Silicon detector unit on the SMART-1 spacecraft. The non-imaging HPSi PIN sensor has a wide field-of-view (FOV) to enable Sun visibility during a significant fraction of the mission lifetime, which is essential for obtaining calibration spectra for the X-ray fluorescence measurements by the imaging D-CIXS spectrometer. The energy range (1–20 keV), spectral resolution (about 250 eV at 6 keV), and sensitivity (about 7000 cps at flux level of  $10^{-4}$  W m<sup>-2</sup> in the range 1–8 Å) are tuned to provide optimal knowledge about the Solar X-ray flux on the Lunar surface, matching well with the activating energy range for the fluorescence measured by D-CIXS. The independent science of the XSM will also be valuable, since the XSM energy range is very sensitive to solar flares. The countrate during the top of an X1 flare will be about 35 times higher than the average quiescent countrate at solar maximum. The relative increase will be the same for an M1 flare during the SMART-1 mission, which will be closer to the next solar minimum. Since the XSM will observe the Sun as a star, and the energy range and spectral resolution are close to those of present astronomical X-ray satellites (e.g., XMM-Newton, ASCA, Chandra), we will obtain an X-ray database of the Sun which can be related with the stellar X-ray observations more easily than the data from present solar X-ray instruments. In this publication we give a detailed description of the design, performance, and tasks of the XSM instrument, and view the science perspectives.

© 2002 Elsevier Science Ltd. All rights reserved.

### 1. Introduction

SMART-1 is a technology demonstration mission of the ESA. It is scheduled for launch as a secondary payload on an Ariane 5 rocket within the time window of a year from October 2002 (Foing et al., 2002). The primary purpose of SMART-1 is to show that the solar electric propulsion system is capable of manoeuvring and thrusting a spacecraft during long deep space missions in the solar system.

SMART-1 will also carry a small scientific and technology payload, including an X-ray instrument for probing and analysing chemical composition of solar system bodies. There is an X-ray instrument presently operating on the NEAR mission of NASA (Goldsten et al., 1997), which has a solid state Si-detector as one of the solar spectrometers while the main X-ray detector observes the surface of the Eros asteroid (Trombka et al., 1997). The SMART-1 X-ray instrument has basically a similar task, with the Moon as the main target. The instrument includes the main detector, D-CIXS (Demonstration of Compact Imaging X-ray Spectrometer) described in detail by Grande et al. (2002), and

\* Corresponding author.

E-mail address: [juhani.huovelin@astro.helsinki.fi](mailto:juhani.huovelin@astro.helsinki.fi) (J. Huovelin).

a calibration detector system, X-ray solar monitor (XSM), which is the subject of the present paper.

## 2. Instrument objectives

The motivation of developing the (XSM) is based on both scientific and technological goals. The science goals are met: (1) via effective use of the mission lifetime for monitoring the solar X-ray activity at all intensity levels in a wide energy range and with a good spectral resolution, and (2) via sufficiently short collection times of individual spectra to allow maximum flexibility in offline analysis of data.

The technology goals are met by mainly concentrating on the development and fine tuning of existing technology, since the schedule for the instrument design and manufacturing is very limited. We also bear in mind the vision for use of a reliable instrument concept in future space science missions, as well as more generic use of solar-flare-warning devices in continuously growing human activity in outer space.

### 2.1. Science goals

The main task of the XSM will be monitoring the direct X-ray flux of the Sun while the D-CIXS is observing the X-ray scattering and fluorescence from the Moon. The XSM data will be needed to calibrate the data of the D-CIXS, since the X-ray flux of the Sun is not constant in time. Examples of such variability in an X-ray spectral range (1–8 Å) covered by XSM are shown in Fig. 1. The intensity of the fluorescence spectrum and the relative strength of lines at different energies depend on the energy distribution of the solar X-ray spectrum which activates the fluorescence (for details, see Grande et al., 2002). Simulated solar X-ray spectra at three different activity levels are shown in Fig. 2 (upper spectra). From the figures it is clear that time-synchronized knowledge of both the intensity and the spectral distribution of the Sun is mandatory for understanding measurements of fluorescence activated by solar radiation. The capability to provide a maximal coverage of time with calibration spectra for the D-CIXS is the main reason for designing a large field-of-view (FOV) for the XSM.

The XSM will be used also for independent science. The spectral range is very sensitive to solar flare activity. During a flare the measured spectrum will be dominated by the flux from the event at energies above 2–3 keV. Although the energy range of XSM does not cover the energies below 1 keV, which is definitely an important region for studies of solar/stellar flares (e.g. Favata and Schmitt, 2000) and also the quiescent corona (e.g. Orlando et al., 2000), the wide energy range above 1 keV will provide very good sensitivity to distinguish variations in flares as well as spectra at quiescence. Examples of our simulations in the full range of solar activity are shown in Fig. 2. Monitoring the evolution

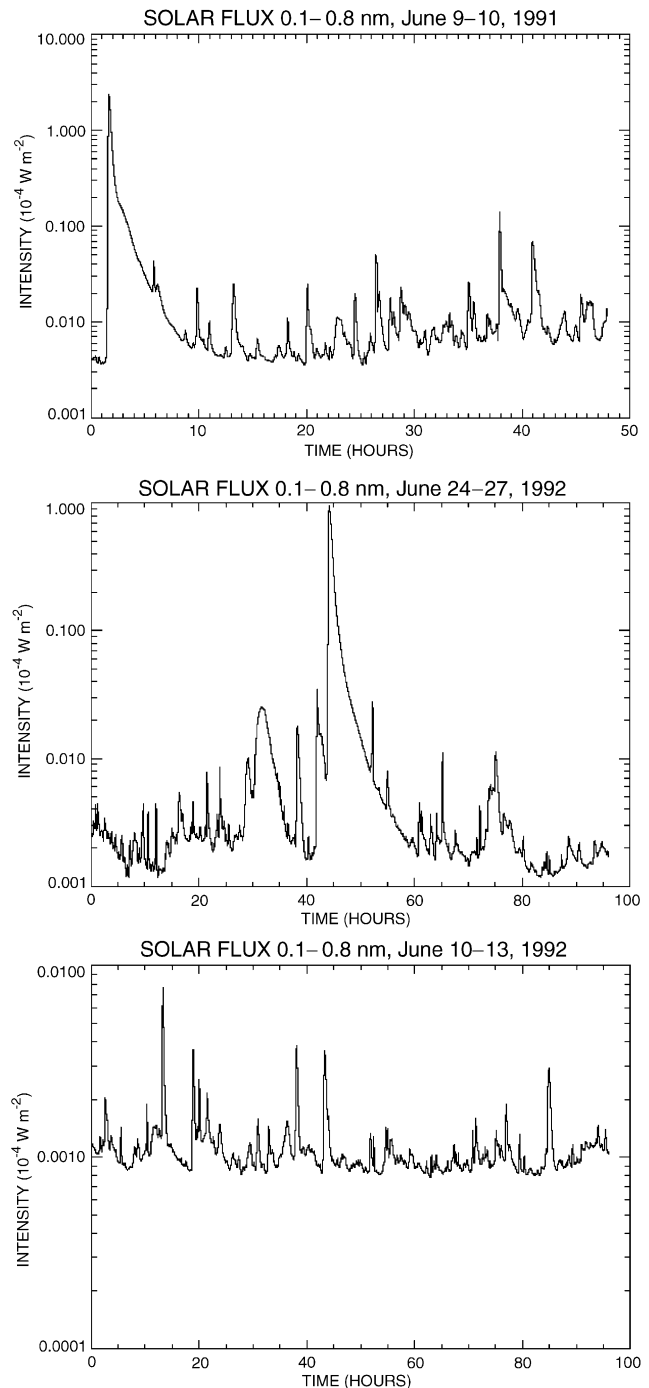


Fig. 1. Solar X-ray flux variations in the spectral range 1–8 Å at three different epochs, which correspond from top to, emission near solar cycle maximum including a large (X3) flare, emission at mid-cycle with flares, and emission of the quiescent Sun at mid-cycle. The data have been extracted from the GOES satellite public WWW archive (<http://spidr.ngdc.noaa.gov:8080/production/html/GOES/goes5min.html>).

of a large number of various flare events during the whole mission will yield a very useful database for general studies of flare physics. Monitoring of the long-term X-ray spectral variability of the Sun has also significance. The XSM can make observations during all the times when the Sun is

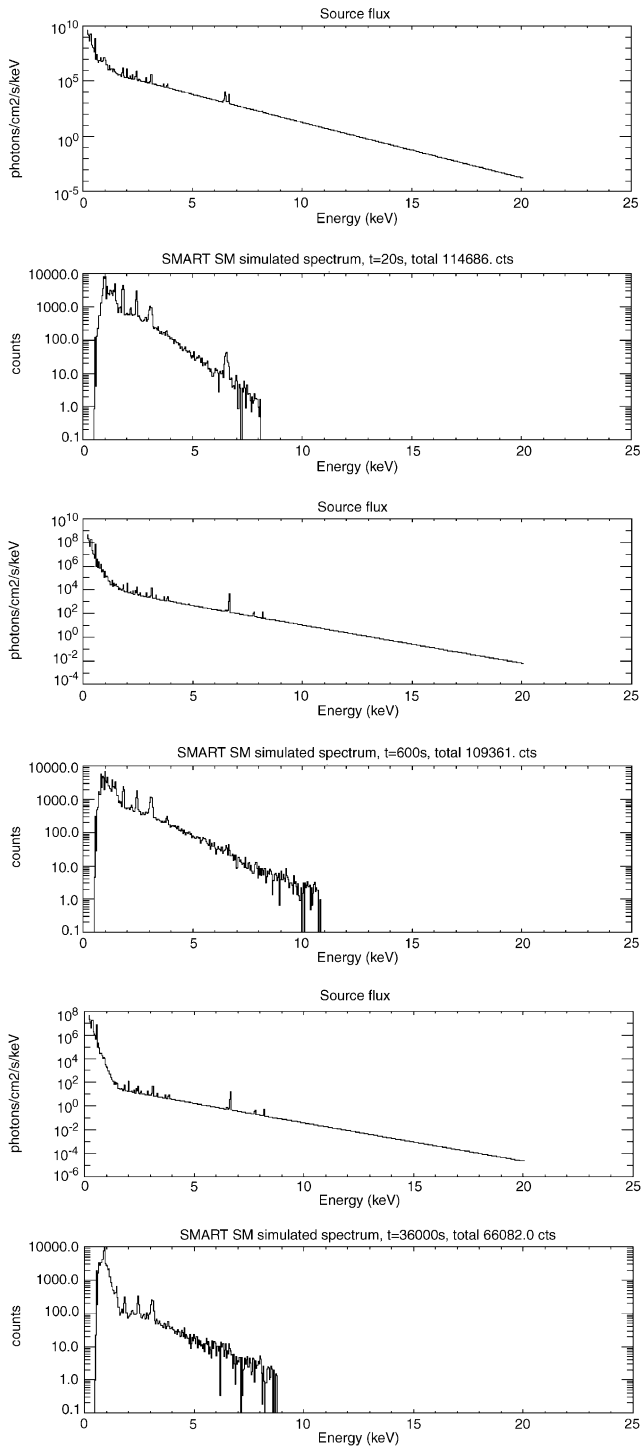


Fig. 2. Simulated X-ray spectra of the full Sun at three different activity levels, which are from top, during an X1 flare at solar cycle maximum, during solar cycle maximum at quiescence, and during solar cycle minimum (upper spectra). The lower spectra show the respective simulated XSM count spectra. The spectrum simulations are based on solar flux data in Zombeck (1990) (see also <http://adsbit.harvard.edu/books/hsaa/index.html>), which have been modelled with multitemperature thin plasma (Raymond–Smith) spectra.

visible for the instrument and power is available, excluding the period after launch with Earth radiation belt passages.

Following the evolution of each flare with a time resolution, which improves with increasing X-ray flux, enables an optimal use of the XSM data for spectral modelling of solar flares. The impulsive phases of strong flares (X-flares) can be traced with spectrum accumulation times down to the minimum of 16 s, and the average quiescent level of solar coronal emission during the planned SMART-1 flight will require integration times of the order of minutes. The XSM will thus be able to trace the whole time evolution of X-ray spectrum during solar flares. The low-energy part (1–10 keV) of the spectra can be fitted with multitemperature thin thermal plasma models, combined with non-thermal (e.g. powerlaw) models for the higher energies near and above 10 keV. These will yield the temporal behaviour of generic physical parameters like temperature ( $T$ ), mean electron density ( $n_e$ ) and emission measure ( $EM \propto n_e^2$ ) during flares. The use of ( $T, n_e$ ) diagram of a flare will enable estimating the heating decay time and further, the physical size of the flare (Reale et al., 1997). Simultaneous space resolved data from, e.g. SOHO, Yohkoh, TRACE, or HESSI will enable comparison with direct observations of flare geometry and dimensions, and by that way it will be possible to improve the flare model applied to the XSM data.

Since the SMART-1 mission lifetime is at least 2 years, the solar activity will change significantly during the mission. Assuming the expected launch time window (2002–2003) the XSM can thus collect very extensive samples of solar X-ray spectra from close to mid-cycle towards the cycle minimum. The solar X-ray spectrum outside flares decreases steeply with increasing energy and becomes very weak at energies above a few kiloelectronvolt. The sensitivity of the XSM enables detection of the solar spectrum from 1 keV to energies above 5 keV with 1 h integration even at the low X-ray emission levels during the solar cycle minimum (see Fig. 3). The instrument will thus be useful also for studying the X-ray emission of the quiescent Sun throughout the solar activity cycle, although the major part of the quiescent flux, which is below 1 keV, is not within XSM's energy range. The higher-energy part of the quiescent coronal spectrum will, in fact, be very interesting in view of a “nanoflare” scenario of solar corona by Parker (1988, 1990) which has later been supported by, e.g., Judge et al. (1998). This scenario suggests that continuously emerging very small flares would be the major energy sources of “quiescent” coronal emission, which implies that the same mechanism would be responsible for essentially all X-ray emission of the Sun. The variations would be caused by different size distribution and surface density of flares at different times. The existence of rapidly variable subarcsecond (i.e. below 700 km) structures in the coronal emission is also supported by Huovelin et al. (2002).

The coronal emission and flare activity of the Sun are known to have strong connection with its magnetic activity

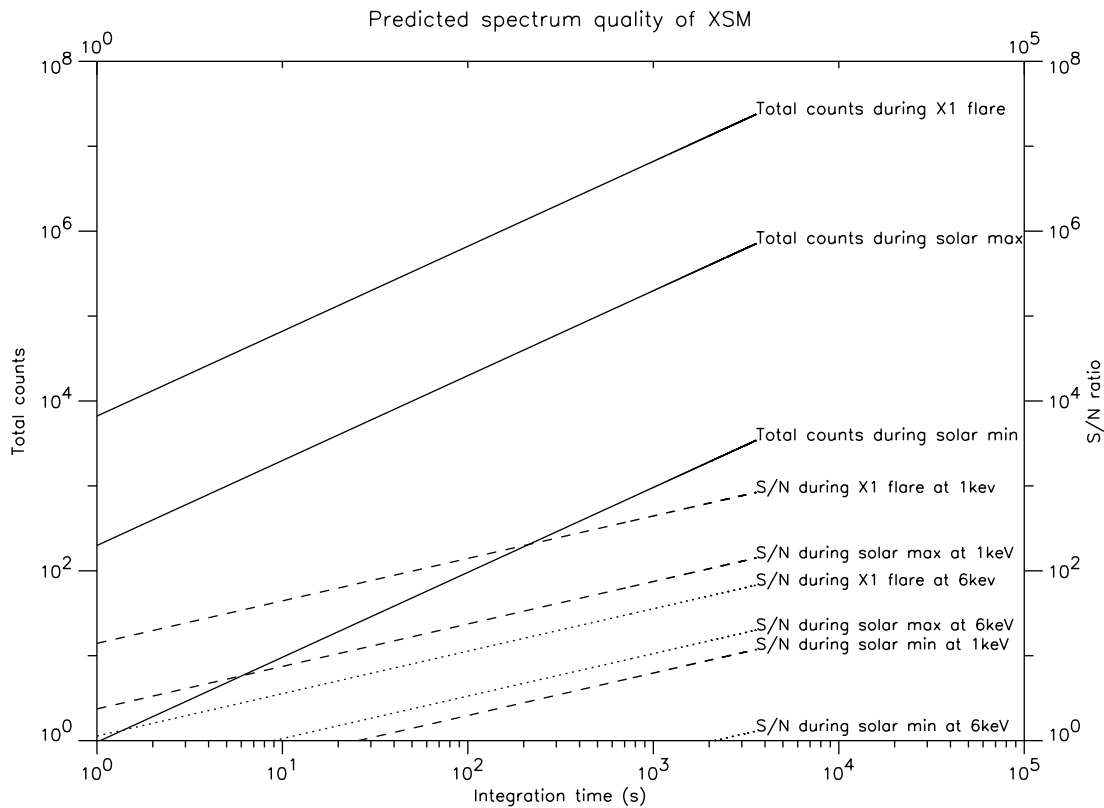


Fig. 3. Sensitivity of XSM. Estimates of expected total counts and  $S/N$  ratios at 1 and 6 keV as a function of integration time for the three cases in Fig. 2.

(e.g. Golub and Pasachoff, 1997). The behaviour of other stars with corona is generally believed to be similar although the coronal temperature and flare activity of other stars is probably somewhat higher than on the Sun (Rosner et al., 1985). The models of the solar corona and flares can thus, in principle, be used for interpretation of stellar X-ray observations. The difficulty in applying observations of the Sun to stars is introduced with differences in the information contents of the observed data. Solar observations usually concentrate on resolving details on the solar surface, and deriving global properties comparable to stellar observations with no spatial resolution is not straightforward (see Peres et al., 2000). A similar observing method for the Sun and the stars would thus be highly desirable also in the X-rays. The XSM will provide a good X-ray database of the Sun, which will be directly comparable to stellar X-ray observations in the range 1–20 keV. It covers the upper energy range of several modern astronomical X-ray satellites (e.g. ASCA, XMM-Newton and Chandra), and their spectral resolution is also close to that of the XSM. Furthermore, the observations of the XSM resemble stellar observations since the XSM sees the whole Sun without spatial resolution, i.e. the Sun as a star.

## 2.2. Technology goals

There are several technology goals and challenges for the design of the XSM. One aim is to design a lightweight and

small instrument with low power consumption. This concept is tempting because of its potential usefulness in future space science missions, and also as a portable radiation detector during manned space activities. The latter use is possible, since the X-rays, being isotropically emitted from a solar flare, provide a reliable warning of a possible increase in energetic particle radiation usually well before the more collimated flare protons and electrons reach the Earth distance from the Sun.

A second aim is to design a detector system, which can be used in a very demanding radiation environment without being permanently damaged by energetic particles (e.g. trapped protons in the Earth's radiation belts). This goal can be, in principle, met in two ways. Either a radiation resistant detector is used, or the detector is shielded against radiation by a mechanical shutter. During the design of the XSM, both of these solutions have been carefully studied. Invoking a shutter mechanism in connection with a well-known detector material, HPSi, has been selected, since a detector made from GaAs or CdZnTe, which would survive the radiation environment better than Si due to the fact that they could be made very thin and absorb less of the harmful protons, would not have the desired energy resolution and energy range. Implementing a reliable and lightweight shutter mechanism for space is one of the challenges in the XSM design.

A third technological goal is to develop a detector which performs sufficiently well near room temperatures, and can

be cooled to the operating temperature with very low power during the most intensive exposure of the sunlight in the space at Earth distance from the Sun. Electric cooling with a Peltier is suitable to reach the required maximum temperature decrease of  $\sim 50^\circ$  with  $\sim 1$  W of power.

A fourth technological goal is to include sufficient signal amplification in the sensor unit before transmitting it with long external cables to the main electronics board in the D-CIXS unit. By our experience, this is the only way to avoid significant signal perturbation due to various uncontrollable sources of noise in cables.

A fifth goal is to maximize the dynamical range of the detector. It should be capable of tolerating high countrates above 10 000 cps without significant signal distortion, and, on the other hand, be sensitive to very low signals at the levels below 1 cps. This requirement comes from the highly variable signal expected from the Sun in the energy range of XSM.

### 2.3. Measurement strategy

Solar X-ray measurements with the XSM can be made, in principle, at all times when the Sun is in the FOV of XSM. The detector will naturally not be operated during the radiation belt passages, but will be allowed to measure during the thrust of the Solar electric power engine.

The XSM provides science data for the data-processing system of the D-CIXS as an event list fed via a large capacity FIFO ASIC developed at the RAL. The energy channel information comes along with each event, and time information with each FIFO packet, which can be read 64 times/s.

The amount of full event data accumulated between successive ground contacts would be too massive to be saved in the onboard memory. Therefore, the event list is processed to X-ray spectra with 512 equally spaced energy channels every 16 s by the D-CIXS onboard software. The binning period is sufficiently short for independent science use of XSM data. Once transmitted to Earth, these data can be used for solar science without loss of scientific value, and can be further binned to reach high enough  $S/N$  ratio required by spectrum analysis. Fig. 3 shows the estimated total counts and  $S/N$  ratios at 1 and 6 keV for cases which extend over the full range of solar X-ray power variations expected during the SMART-1 mission.

The plan is to start observations after SMART-1 orbit has grown above the Earth's radiation belts, indicating that first observations will be made about 80–100 days after launch. After that, observations will be conducted during the cruise phase of SMART-1 with an upper limit set by two constraints, the spacecraft attitude, and the leakage current of the Si PIN detector. Due to the effect of, e.g., D-CIXS cruise phase pointings, a detailed timeline for XSM observations in yet to be defined. As a rough estimate, however, it is certain that XSM observations will be possible for more than

50% of the SMART-1 cruise phase time. The leakage current monitoring, and possible limiting of observing time to minimize the corrupting effects of space radiation, is necessary to ensure sufficiently good spectral resolution during the Moon orbiting phase. The procedures for this, i.e. keeping the detector shutter closed during high levels of particle radiation and annealing to restore the performance, will probably decrease the effective observing time by 1–2% at most.

The total observing time with XSM during the cruise phase of SMART-1 will thus be 175–220 days (15–19 million s) depending on the actual duration of the cruise phase (15–18 months). The Sun visibility for the XSM will also be maximized via spacecraft manoeuvring during Lunar orbiting, and therefore the expected observing time will be more than 50% of the total Lunar orbiting phase of 6 months, which will lead to a total observing time of at least 285–310 days (roughly 22–26 million s) during SMART-1 mission. We studied the public GOES data at WWW (Space Physics Interactive Data Resource/National Geophysical Data Center) taken during the decay of last solar cycle (August 1992–August 1996) to predict the coverage of flare activity during SMART-1 mission. As can be expected, the decay of the cycle has a very significant effect on the X-ray flux level of the Sun, and the number of strong flares diminishes dramatically during 1 year shift in time. As a rough estimate, which allows large flexibility for launch dates, we took the fractions of time during 1000 days from August 1992 where the X-ray flux in the 1–8 Å band exceeded levels  $10^{-6}$  (C1),  $5 \times 10^{-6}$  (C5),  $10^{-5}$  (M1),  $5 \times 10^{-5}$  (M5), and  $10^{-4}$  (X1) W/m<sup>2</sup>. From these, the expected times above flare levels C1, C5, M1, M5, and X1 during the XSM observations will be 470, 50, 20, 3, and 1 h, respectively. The average number of various flares in the period will decrease from a daily average of 10, in the beginning of SMART-1 mission, to a daily average of 4 in the end, and the total number of flares observed with the XSM will thus be about 2000.

## 3. General description of the instrument

The XSM is technically a subsystem of the D-CIXS. The instrument receives its power and commands via the D-CIXS and transfers all signals and data to the D-CIXS. Since the XSM sensor is designed to have an optimal field of view towards the Sun, it will be mounted on the +X panel of SMART-1, while the D-CIXS is mounted on the opposite –X panel. The XSM sensor unit is connected with a cable to an electronics board installed in the D-CIXS unit. The block diagram of the main parts is schemed in Fig. 4.

The sensor box of aluminium contains a HPSi diode, a Peltier cooler, pre-amplifiers, shaping amplifiers, and a small shutter mechanism. The sensor unit is shown in Fig. 5. The box is attached at an angle of  $45^\circ$  with respect to the spacecraft +X panel with a support bracket.

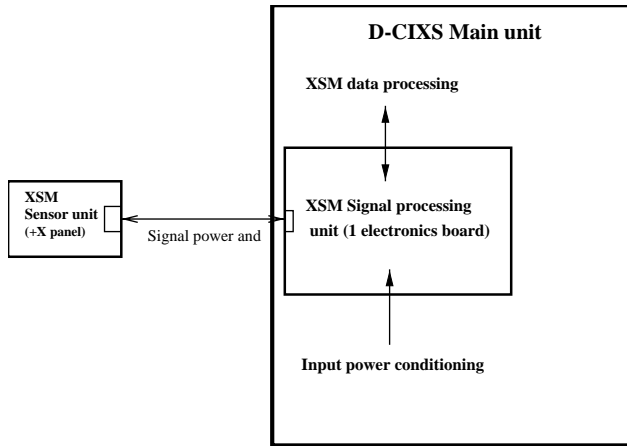


Fig. 4. A block diagram showing the major components of the XSM system.

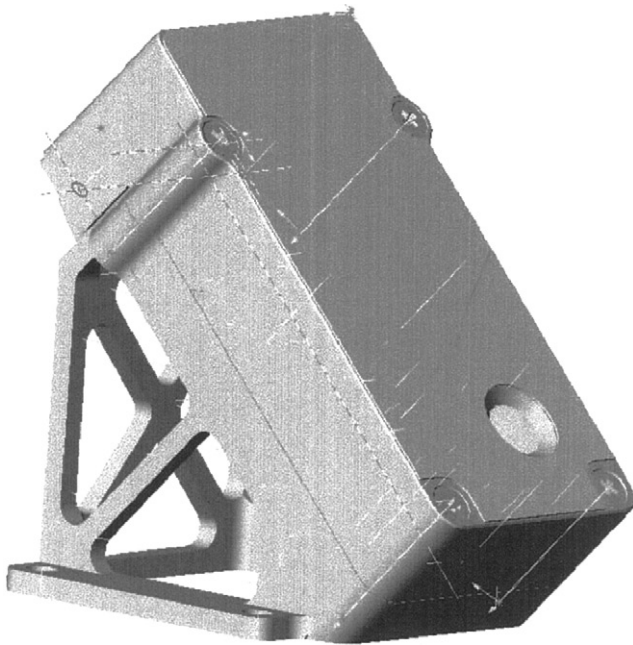


Fig. 5. The XSM sensor unit box with supporting bracket. The dimensions of the box are 26/40/80 mm ( $H/W/L$ ), and tilting by the bracket is  $45^\circ$ .

To avoid extensive heating of the XSM sensor unit, its reflectivity must be optimized. This is accomplished by attaching a second surface mirror (SSM) tape on the front cover plate which thus acts as an additional radiator/passive cooler. The sides of the sensor box are shielded under a multilayer insulator (MLI) blanket, similar to that of the whole SMART-1 spacecraft.

The XSM electronics board in the D-CIXS unit is a multilayer Eurocard, which contains AD and power converters, and electronics for transmitting the science data, housekeeping, and control signals. Due to the dominating role of the Sun in the output of X-rays at Earth distance from the Sun, there is no telescope to focus the solar signal for the XSM,

and the FOV of the detector is maximized by making the opening angle of the XSM detectors as wide as possible.

### 3.1. Detector

The detector is based on a  $500\ \mu\text{m}$  thick HPSi PIN diode, mounted on a ceramic substrate together with front end amplifiers and a temperature sensor. The substrate is sitting on top of a two-stage Peltier cooler (able to cool down the diode and transistors below  $-20^\circ\text{C}$  from an ambient temperature around  $+40^\circ\text{C}$ ) and this whole assembly is mounted in a hermetic package which contains a  $25\ \mu\text{m}$  thick Be-window on a  $\sim 1\ \text{cm}$  diameter circular opening. The small distance of the detector to the window, together with a large  $D/d$  ratio for the window diameter ( $D$ ) and the detector aperture ( $d$ ) enables a large FOV. The size of this package is less than a thumbnail (in cross section) and it weighs less than 5 g. The detector package structure is shown in Fig. 6.

### 3.2. On board control and processing

The signal processing circuitry in a sensor box consists of a preamplifier, a shaping amplifier, and a baseline restorer. The shaped signal will be transferred via an external cable to the main board in the D-CIXS unit for pulse height analysis. The system dead-time will be very small (a few tenths of a microsecond) due to the implementation of loss-free counting (Westphal, 1979). The AD-converted pulses will be stored in a FIFO memory and read out by the system (D-CIXS) microprocessor 64 times a second. This microprocessor will also be in charge of sending commands and receiving housekeeping data. Commanding is handled by an 8 bit register and housekeeping output by a 16-bit AD converter, both tied to the D-CIXS backplane. Further processing of the signals and data by the D-CIXS system is explained in detail by Grande et al. (2002).

## 4. Calibrations

The energy resolution and the channel vs. energy relation of the detectors will be calibrated before flight with a special setup which is being designed for the XSM in the X-ray Laboratory, University of Helsinki. The setup will include an X-ray tube as the source, a monochromator crystal, an adjustable collimator to limit the beam size, and a computer-controlled  $X-Z$  table for adjusting the position of the calibrated detector. The calibration in low X-ray energies (below 5 keV) is not possible in air at normal pressure, since the input radiation at the lowest energies (near 1 keV) would be totally absorbed in a few centimetre. Therefore, either a vacuum, or an atmosphere of some transparent gas has to be arranged for the X-ray path. In the case of the XSM calibration, a dedicated system with a vacuum chamber will be used.

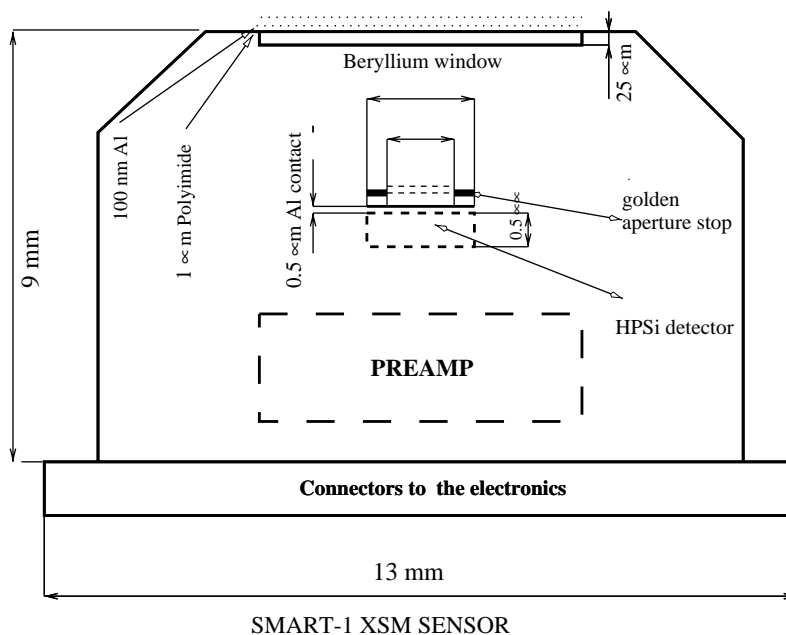


Fig. 6. XSM detector package structure.

Table 1  
Characteristics of the XSM

Mass/sensor box	~ 0.17 kg
$H \times W \times L$ of sensor box	$26 \times 40 \times 80 \text{ mm}^3$
<i>Sensor features</i>	
Detector material	HPSi (high-purity silicon)
HPSi crystal thickness	0.5 mm
Detector diameter	2 mm
FOV diameter	$105^\circ$
<i>X-ray window and other filtering</i>	
Beryllium window	25 $\mu\text{m}$
Silicon dead layer	~ 200 nm
Aluminium contact layer	500 nm
Aperture stop (Au) thickness	125 $\mu\text{m}$ (inner radius 0.75 mm)
<i>Setup</i>	
Energy range	1–20 keV
Number of channels	512 (~ 40 eV/channel)

The XSM detection efficiency will be studied and characterized in absolute scale with the aid of a second solid-state detector for which the detection efficiency is known precisely enough. The XSM efficiency is thus obtained by comparing the white-beam spectra from a medium-Z X-ray tube acquired with both detectors. Also the performance of the loss-free counting scheme under extreme countrate conditions can be tested in a reliable way as the white-beam spectrum of an X-ray tube is well known, and pile-up effects in the output spectrum shape with increasing countrate can be seen in a continuum spectrum covering the whole energy range. (Table 1).

The accuracy of the absolute flux attainable with this scheme is of the order of 1 percent or better. Considering the expected flux levels and sensitivity of the instrument, statistical errors in the measured count spectra will be bigger for each 16 s integration, and D-CIXS fluorescence calibrations with the XSM can be made assuming an error limited by photon statistics. As for the independent coronal science with the XSM data, the above absolute flux calibration is more accurate than the uncertainty due to background radiation, which will probably be the dominating source of error in long integrations of the solar X-ray spectrum.

The effective area of the detector depends on the solar aspect angle, since the projected path length of the X-ray photons through the filters and the projected thickness and area of the detector depend on the viewing angle. The effective area of the XSM will be calibrated in laboratory for the full range of solar aspect angles ( $0\text{--}52^\circ$ ) using the setup for absolute calibration, where the detector can be adjusted to arbitrary angles with respect to the incoming beam.

The in-flight energy (i.e. channel vs. energy) calibrations will be made using the observed solar X-ray spectra, which includes coronal emission lines with known energies and the characteristic absorption edges of the detector system (e.g., the silicon edge at about 1.8 keV).

The quantum efficiency of the detector and channel vs. energy relation are expected to be very stable during the whole mission, while the energy resolution will probably be degraded due to permanent changes of the Si crystal lattice by energetic cosmic and solar particle (mainly proton) radiation. This effect can be seen directly by measuring the leakage current of the detector. The consequent increase of the spectral line widths can be estimated from on-ground

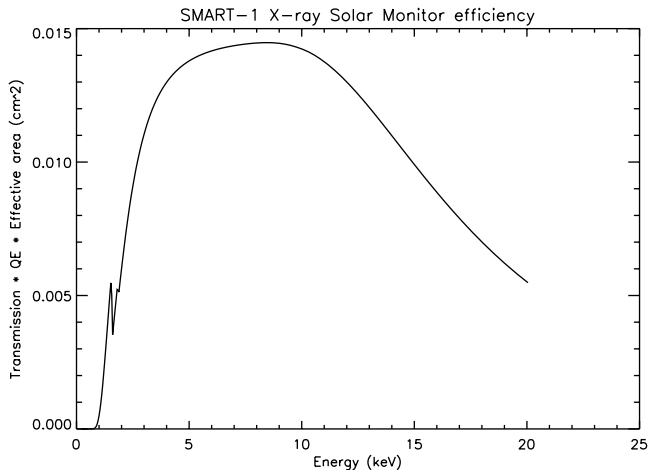


Fig. 7. The on-axis effective area of XSM detector, including the effects of the filtering materials, and the detector quantum efficiency multiplied by the geometrical area of the active detector.

calibrations of a test detector, and will also be checked from observed spectra. Our predictions have shown that the resolution change during the whole mission may be about 100 eV at 6 keV (from about 250–350 eV) at maximum, and the effect will be minimized by heating the detector in regular intervals (once per 2–4 weeks) to about 100°C. According to our tests, an optimal time for each annealing procedure is 4–6 h for the XSM detector. The annealing will also remove additional surface leakage current caused by electron radiation in space. The effect of electrons is much smaller than the effect observed in the Si-PIN detector at NEAR mission (Starr et al., 1999), since the XSM Si-PIN design is different and less sensitive to this effect than the one at NEAR.

## 5. Performance

The XSM has a wide spectral range (1–20 keV) and good energy resolution (250 eV at 6 keV). Fig. 7 shows the effective area of the detector including the transmissions of the filtering materials, the detector quantum efficiency, and the detector area. The detector does not have spatial sensitivity, and thus the Sun is observed as a star. The FOV of the sensor is  $\sim 52^\circ$  symmetrically around the optical axis, which means that the detector will see about 1/5 of the whole sky. The sensor can collect X-ray events at very high countrates with negligible loss and minimal spectral distortion (e.g. 20 000 cps with 1% pile-up). The dead-time is minimized by using the fast channel ( $< 500$  ns) as the primary event counter (Westphal, 1979).

The estimated solar countrate with XSM during the maximum of an X1 flare is 7000 cps, during the quiescent state at solar cycle maximum 200 cps, and during the cycle minimum 1–2 cps (see Fig. 2, lower spectra, and Fig. 3). According to our estimate, which is based on the sky emission

including all X-ray sources, the sky background will be  $\sim 0.2$  cps. Due to the small effective detector area (1.8 mm<sup>2</sup>), the expected instrumental background is lower than the sky background. The background will thus contribute only 10% of the measured signal even at the lowest expected solar emission during the cycle minimum.

## 6. Measurements, reductions and analysis

The measurements will be similar in all cases, since technically the detector will have only one measurement mode. In this mode the high voltage (detector bias) and the detector cooling are set on, and the detector operates as an X-ray photon counter. The signal is processed using a fast channel for the timing and a slow channel for the energy measurement of the absorbed photons. After an AD conversion, the event data (energy of each event) is buffered to D-CIXS in 1/64 s intervals, where the data is finally sampled to energy spectra. The spectrum construction will be made by the D-CIXS onboard processor in 16 s intervals. The collected energy spectra including the associated header data will be transmitted via a CAN bus to SMART-1 for transmission in 4 day intervals to the ground station. The spectrum reductions and further science analysis will be made offline, partly by instrument specific software developed by the instrument team, and partly by using public packages for astronomical X-ray spectral analysis (e.g. XSPEC/XANADU). The XSM data will be archived in flexible image transport system (FITS) format.

## 7. Collaborating institutes and Co-Is

The XSM detector project is co-ordinated by science teams at the Observatory and at the X-ray Laboratory of the University of Helsinki. The XSM detector is being built in Finland by Metorex International. The principal investigator of XSM is Dr. Juhani Huovelin from the Observatory, University of Helsinki, Finland, and the PI of D-CIXS is Dr. Manuel Grande from the Rutherford Appleton Laboratory, UK. Due to the XSM being part of the D-CIXS/XSM X-ray instrument complex, the teams in Finland and in UK work in close collaboration.

The Finnish D-CIXS/XSM science team has six Co-Is, Dr. Pasi Hakala from the University of Turku, and Drs. Keijo Hämäläinen, Jarkko Laukkanen, Karri Muinonen, Jukka Piironen, and Osmi Vilhu from the University of Helsinki. Associated scientists of the project are Lauri Alha (M.Sc.(Eng.)) and Panu Muhli (M.Sc.) from the University of Helsinki, and Hans Andersson (M.Sc.(Eng.)) from Metorex International.

## Acknowledgements

The XSM project is financially supported by the Technology Development Centre TEKES (hardware design and

manufacturing) and the Academy of Finland (Grant No. 47206 for scientific research).

## References

- Favata, F., Schmitt, J.H.M.M., 2000. *Astronom. Astrophys.* 350, 900.
- Foing, B., et al., 2002. *Planet. Space Sci.*, these proceedings.
- Goldsten, J.O., McNutt Jr., L.R., Gold, R.F., et al., 1997. *Space Sci. Rev.* 82, 169.
- Golub, L., Pasachoff, J.L., 1997. *The Solar Corona*, 1st Edition. Cambridge Univ. Press, UK, ISBN 0 521 48082 5.
- Grande, M., et al., 2002. *Planet. Space Sci.*, these proceedings.
- Huovelin, J., Pohjolainen, S., Vilhu, O., Virtanen, J., Kurdt, W., 2002. SOHO/SUMER Observations of Solar X-ray Bright Points. *Mon. Not. R. Astron. Soc.*, in preparation.
- Judge, P., Hansteen, V., Wikstol, O., Wilhelm, K., Schühle, U., Moran, T., 1998. *Astrophys. J.* 502, 981.
- Orlando, S., Peres, G., Reale, F., 2000. *Astrophys. J.* 528, 524.
- Parker, E.N., 1988. *Astrophys. J.* 330, 474.
- Parker, E.N., 1990. *Mechanisms of Chromospheric and Coronal Heating*. In: Ulmschneider, P., Priest, E.R., Rosner, R. (Eds.), Springer, Berlin, pp. 615.
- Peres, G., Orlando, S., Reale, F., Rosner, R., Hudson, H., 2000. *Astrophys. J.* 528, 537.
- Reale, F., Betta, R., Peres, G., Serio, S., McTiernan, J., 1997. *Astronom. Astrophys.* 325, 782.
- Rosner, R., Golub, L., Vaiana, G.S., 1985. *Annu. Rev. Astron. Astrophys.* 23, 413.
- Starr, R., Clark, P.E., Evans, L.G., et al., 1999. *Nucl. Instr. and Meth. A* 428, 209.
- Trombka, J.I., Floyd, S.R., Boynton, W.V., et al., 1997. *J. Geophys. Res.* 102, 23 729–23 750.
- Westphal, G.P., 1979. *Nucl. Instr. and Meth.* 163, 189.
- Zombeck, M.V., 1990. *Handbook of Space Astronomy and Astrophysics*, 2nd Edition. Cambridge Univ. Press, UK, ISBN 0 521 34550 2.